Finite-Volume Time-Domain Analysis of a Cavity-Backed Archimedean Spiral Antenna

Christophe Fumeaux, *Member, IEEE*, Dirk Baumann, *Student Member, IEEE*, and Rüdiger Vahldieck, *Fellow, IEEE*

***Abstract*—This paper presents a comprehensive analysis of a broadband (2–18 GHz) cavity-backed Archimedean spiral antenna. The simulation of the device is performed using the finite-volume time-domain method. The high geometrical flexibility of this method permits a detailed modeling of the antenna including the thin substrate, the feeding balun, and the cavity loaded with a honeycomb absorber. The simulated far-field radiation patterns and the return loss are compared to measurements, showing an excellent agreement over the whole frequency band. The radiation mechanism of the spiral is visualized by observing the current distribution on the spiral arms for both pulsed and harmonic excitation modes.**

***Index Terms*—Current distribution, spiral antennas, time domain analysis.**

I. Introduction

PLANAR spiral antennas are widely used as circularly polarized broadband devices for airborne RF applications. They are compact, can be flush-mounted on the surface of a vehicle and are characterized by stable input impedance and radiation characteristics (gain, axial ratio, beamwidth) maintained over several octaves. Because of the front-to-back symmetry, a spiral antenna in free space radiates bi-directionally, i.e., with maxima on each side of its plane. Therefore, for most applications, where unidirectional operation is required, the spiral is backed by an absorber-loaded cavity. This eliminates back-side radiation without decreasing the frequency band of operation, however at the cost of an efficiency reduction. The wideband balun necessary for the balanced feeding of the antenna is commonly embedded in this cavity. The frequency band of the spiral as a circularly polarized radiator is limited by the following dimensions: The outer radius of the spiral sets the lower frequency of operation, whereas the extent of the feed determines the high-frequency limit.

The analysis of cavity-backed spiral antennas represents a complex problem, that is not easily handled by numerical methods. This has been shown by several authors who have investigated different types of spirals using various computational techniques (e.g., [1]–[7]). Among the different spiral types, the Archimedean spiral is often found in practical systems. It is characterized by a constant arm width. Stable radiation characteristics over large bandwidths are obtained using tightly wrapped spirals, i.e., with narrow arms and a large number of windings. Each spiral arm exhibits consequently a very large length/width ratio.

The accurate modeling of such features, which represents a very challenging problem in computational electromagnetics, is addressed in the following using the finite-volume time-domain method (FVTD) [8], [9]. An essential characteristic of the FVTD method is its geometrical flexibility, since the discretized equations are solved in unstructured inhomogeneous meshes. Therefore, the method is well suited for electromagnetic problems involving curved surfaces and different scales of structural details.

In this paper the FVTD method is applied to the analysis of a cavity-backed Archimedean spiral antenna for operation between 2 and 18 GHz. The discretized model of the device exhibits a remarkable level of details, including the width of the spiral arms, the thin substrate, the absorber-loaded metallic cavity and the feeding mechanism (balun). For validation of the method, the return loss and the far-zone radiated patterns obtained from the simulations are compared with measurements performed in an anechoic chamber, showing an excellent agreement. The results of the time-domain simulations further permit visualization of the current densities on the spiral arms, either in pulsed or harmonic operation. This allows insight into the radiation mechanism of the device, illustrating the well-defined frequency-dependent active zone of the spiral.

II. FVTD Spiral Antenna Model

In the following, the relevant simulation characteristics of the spiral antenna are presented. After a short description of the method applied, the investigated device is depicted in three steps: The spiral itself, the feed and the absorber loaded cavity.

A. The FVTD Algorithm

The FVTD formalism is based on the following volume-surface integral forms of Maxwell's curl equations [10], [11]

$$-\frac{\partial}{\partial t}\iiint_{V_i}\vec{B}dv=\oiint_{\partial V_i}\vec{n}\times\vec{E}da$$
$$\frac{\partial}{\partial t}\iiint_{V_i}\vec{D}dv=\oiint_{\partial V_i}\vec{n}\times\vec{H}da. \quad (1)$$

In this equation, the integration volume V_i is bounded by the surface ∂V_i and $\vec{n}$ represents the outward-pointing normal unit vector of the surface element da. The coupled equations in (1) need to be discretized for computation of a numerical solution. Several variations of the FVTD scheme exist, based on different locations of the variables and various approximations used in practical implementations [12]. The algorithm of the present

Manuscript received June 24, 2005; revised October 7, 2005. This work was supported by Armasuisse, Science and Technology, Bern, Switzerland.

The authors are with the Laboratory for Electromagnetic Fields and Microwave Electronics (IFH), ETH Zurich, 8092 Zürich, Switzerland (e-mail: fumeaux@ifh.ee.ethz.ch).

Digital Object Identifier 10.1109/TAP.2006.869935

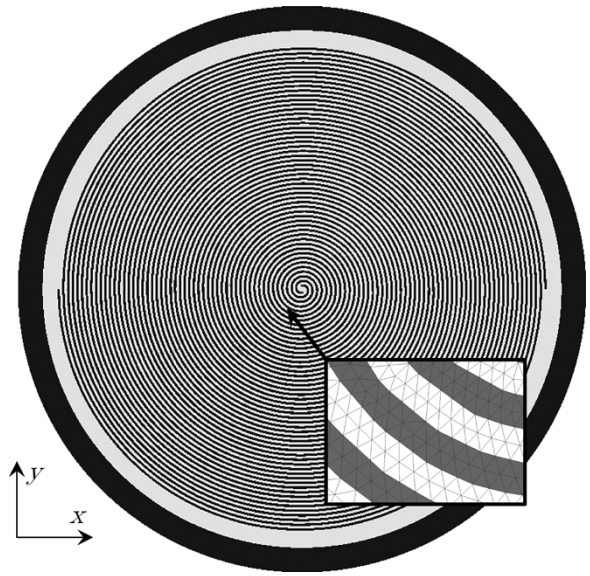

Fig. 1. Top view of the spiral antenna. The metal parts are shown in black. The outer ring corresponds to the top of the metallic cavity. The light gray corresponds to the substrate. The inset shows a magnification of the surface mesh of the spiral.

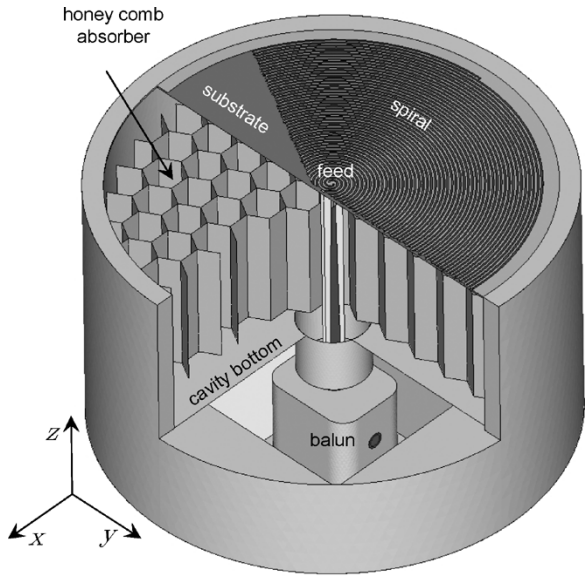

Fig. 2. Cut open FVTD model of the spiral antenna showing the arrangement of the spiral, the substrate, the cavity loaded with the honeycomb absorber, and the balun.

analysis is applied in a tetrahedral meshed and is based on a cell-centered flux-splitting formulation together with the monotonic upwind scheme for conservation law (MUSCL) [11]. The time discretization follows a Lax-Wendroff predictor-corrector time iteration [11], coupled with a local time-stepping scheme [12]. The inhomogeneity of the space discretization (tetrahedral mesh) permits to minimize the number of cells necessary to model a complex multi-scale structure, whereas the geometry-matched local time steps relax the stability criterion, increasing the efficiency of the algorithm.

B. FVTD Model of the Spiral

An Archimedean spiral is characterized by a fixed arm width along its windings. The spiral function can be written in polar coordinates (ρ, ϕ) as

$$\rho = \rho_0(\phi + \phi_0) \tag{2}$$

where ρ_0 defines the winding tightness and ϕ_0 is the starting angle of the spiral which determines the inner radius. A two-arm self complementary spiral antenna is defined by rotating 4 such curves in increments of $\pi/2$. The cavity-backed spiral antenna investigated here is an existing device designed for 2–18 GHz. The spiral arms start at an inner radius equal to 0.25 mm, necessary to accommodate the space for the feed. The full spiral structure, with 26 turns and an outer radius of 26 mm, is shown as top view in Fig. 1. The metallic spiral arms are supported by a substrate with thickness 0.254 mm and a relative dielectric permittivity $\varepsilon_r = 2.2$. This thin substrate is included in the FVTD model and its role will be discussed in Section IV-C.

The geometry of the spiral puts stringent requirements on the model discretization: Besides the difficulty of modeling the curved spiral shape, the structure exhibits large differences in scales, since the overall length along one arm of the spiral is more than 2 m, whereas the transversal arm width is only 0.25 mm (length to width ratio $>$ 8000). An unstructured, inhomogeneous mesh is a then great advantage to model the spiral antenna with a minimum number of volume elements: The typical linear size of the tetrahedron increases rapidly with the distance to the spiral, from $\sim \lambda_{\min}/100$ necessary to resolve the feed, to $\lambda_{\min}/10$ commonly required for free-space FVTD simulations.

C. FVTD Model of the Feed

The cavity-backed spiral antenna is connected to the outer electronics through a coaxial connector. A broadband balun transforms the unbalanced coaxial mode into the balanced two-wire transmission line mode that feeds the antenna. Additionally, the balun provides impedance transformation (through a tapered paired-strip line), from the 50 Ω impedance of the coaxial line to the impedance of the spiral antenna. The balun is inserted in the cavity that backs the spiral. The corresponding analysis, in particular the general definition of the ports in the FVTD algorithm, has been addressed in [13]. In the following simulation, the balun is included in the full model of the spiral antenna.

D. FVTD Model of the Absorber-Loaded Cavity

The absorber-loaded cavity behind the spiral suppresses undesired back radiation of the spiral. The cavity (around 22 mm deep) is filled with a honeycomb absorber with hexagonal cells arranged as shown in Fig. 2. The honeycomb structure itself is coated with a resistive material. The resistivity is graded, with an increase toward the bottom of the cavity to maximize absorption. Obviously, the absorber lowers the efficiency of the antenna by about 50%.

To model the absorber-loaded cavity in FVTD, the resolved honeycomb structure is considered as made of thin conducting sheet. The conductivity is increased in two successive steps in the lower part of the cavity to reproduce the graded coating of the honeycomb absorber. Surface impedance values, required

for the numerical analysis, are approximated on the basis of reflection and transmission measurements performed in waveguides loaded with the honeycomb absorber. Parametric simulations indicate that the reflection and transmission are not critically sensitive to parameter variations.

E. Computational Load

The convergence of the simulation has been tested using different surface discretization of the spiral arms. Good convergence of the results is observed when at least two rows of triangles per arm width are used, as shown in the inset of Fig. 1. Based on the surface mesh, a strongly inhomogeneous volume mesh is created with rapidly growing tetrahedrons around the spiral. The resulting full model shown in Fig. 2 requires 1.5 millions tetrahedrons, which translates into a memory requirement of around 1 GB, compatible for use on a standard PC. For a simplified spiral model, for example for a spiral in free-space, the memory requirements can be decreased under 700 MB. In all cases, the heaviest part of required memory lies in the resolution of the spiral itself.

The volume ratio of the largest to the smallest cell is around 600'000, and the use of geometry-matched local time steps [12] is then crucial to increase the efficiency of the FVTD computation: The tiny cells necessary to resolve the spiral arm structure and the spiral feed require a very short time step ($\sim$0.04 ps), whereas the largest cells of the present model are updated up to 32 times less often.

The time-domain analysis of the spiral requires very long simulation times in order to allow low-frequency components to propagate along the spiral arms out to their radiation region, as will be shown in the next section. Simulation times of 10 ns are considered necessary for convergent results down to 2 GHz. This requirement translates into large overall CPU times: The computation times for the most sophisticated model required several days (on average 5 s per time step Δt) on a standard Pentium IV computer, which are comparable to the data given in [6] obtained with FDTD for a spiral in free-space. Currently tested acceleration techniques for the FVTD code are expected to yield a significant improvement of the computational efficiency.

The next two sections describe the results of the numerical analysis. First, a comparison of the simulated radiation performances with measurements will be presented. Second, the current densities on the spiral arms will be discussed.

III. Comparison With Measurements

A validation of the presented simulations is obtained by comparison with measurements. For this purpose, the far-field patterns and the return loss of the antenna have been measured over the whole operation range.

A. Far-Field Pattern

Fig. 3 compares measured and simulated patterns at 2, 4, 8, and 16 GHz in two orthogonal planes xz and yz perpendicular to the spiral plane (see Fig. 2). The selected frequencies are representative of the very good agreement in the whole frequency range of operation.

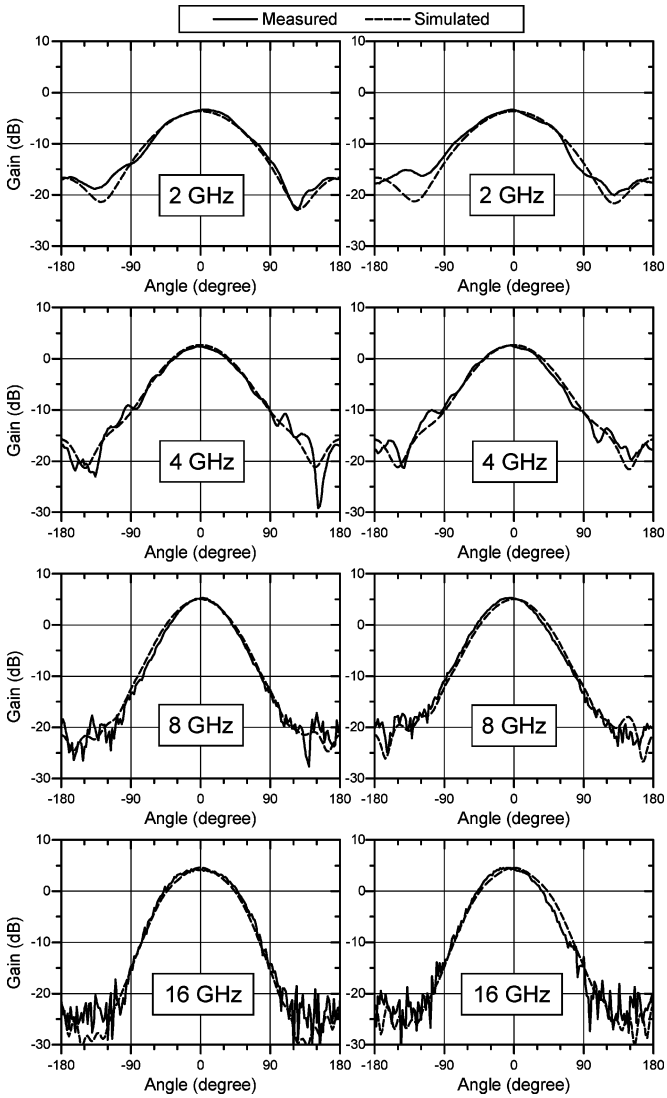

Fig. 3. Measured and simulated far-field patterns of the cavity-backed spiral at the four featured frequencies in two orthogonal planes perpendicular to the spiral plane: —— measured, – – – simulated. LHS: xz plane, RHS: yz plane.

The axial ratio (AR) and the phase between the two orthogonal electric field components E_ϕ and E_θ are shown (for the same frequencies) in Fig. 4, limited to one plane for brevity. The phase of 270 degree observed for back radiation indicates a reversal of polarization for back radiation.

Through all the operating frequency range of the spiral antenna, its polarization is circular, with an axial ratio well under 3 dB in broadside direction. Fig. 5 shows, as a function of frequency, the simulated broadside axial ratio together with the phase $\Delta\varphi$ between E_ϕ and E_θ. Both the axial ratio and the phase clearly indicate the transition from linear polarization ($\mathrm{AR} = \infty$, $\Delta\varphi = 0°$) to circular polarization ($\mathrm{AR} = 0$ dB, $\Delta\varphi = 90°$), which happens slightly below 2 GHz. At this frequency of operation, currents reflected at the outer end of the spiral arms alter the circular polarization of the spiral.

As will be demonstrated later (Section V), the thin substrate decreases the effective wavelength of the currents on the spiral arm. Therefore, the presence of a substrate shifts slightly the bandwidth of the spiral toward lower frequencies.

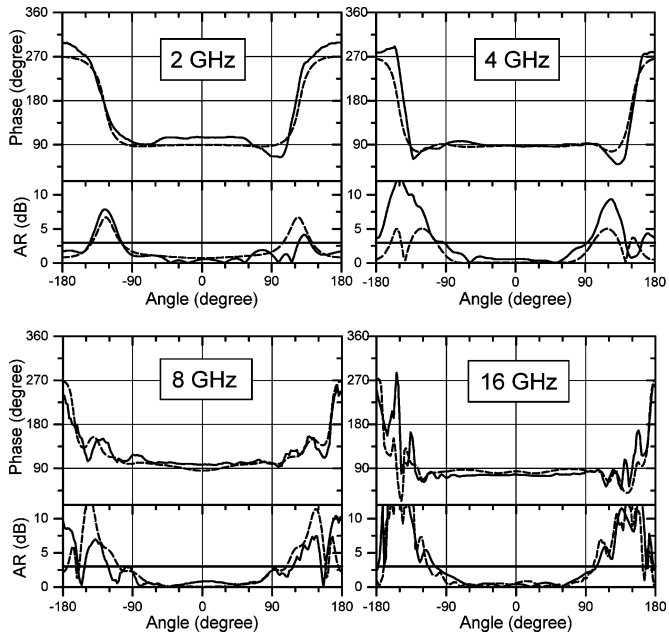

Fig. 4. Measured and simulated axial ratio (AR) and phase between the two orthogonal components E_ϕ and E_θ in the xz plane. —— Measured, – – – simulated.

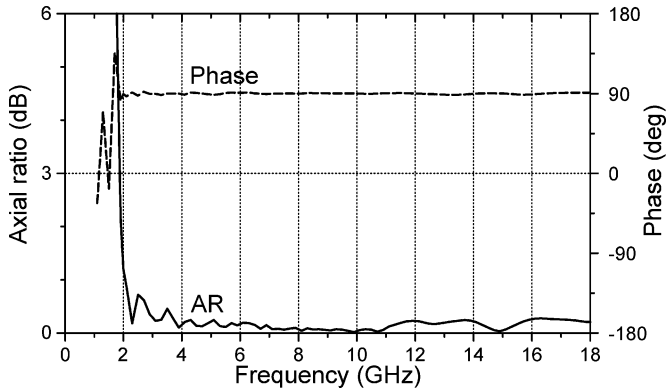

Fig. 5. Simulated broadside axial ratio of the polarization ellipse and phase between the orthogonal field components as a function of the frequency. The two curves illustrate the transition from linear to circular polarization (occurring below 2 GHz).

B. Return Loss

A simulation of the balun and the feed mechanism for the spiral antenna has been presented in [13]. In this reference, the two-wire line that feeds the spiral was terminated with an absorbing boundary. Simulating the balun embedded in the full spiral antenna yields a very similar matching behavior. This is demonstrated in Fig. 6, where both simulated results are compared and good agreement to the measured return loss of the spiral antenna was found. The results show merely a slightly higher reflection in the region of low return loss S_{11} for the full device compared to the isolated balun. This indicates that the balun is the component that mostly determines the return loss and therefore plays the most critical role to achieve broadband operation of a practical spiral. Simulations of the balun and of the spiral structure might be carried out separately to save computer resources, at the cost of a slightly reduced accuracy.

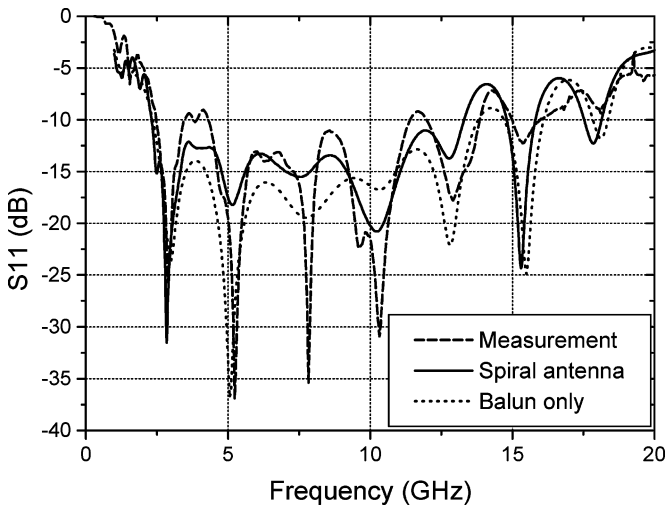

Fig. 6. Comparison of the simulated and measured return loss of the cavity-backed spiral antenna. Also represented is the return loss of the balun only.

IV. Current Density Distribution on the Spiral

The representation of the current distribution on the arms of the spiral permits to visualize the active region of the spiral radiator. The surface electric current densities on the spiral arms are retrieved from the near-zone field distribution. The sign of the current density is determined from its component tangential to the spiral according to the following convention:

- positive for currents along the spiral toward the outer end;
- negative for currents along the spiral toward the feed.

In the following, the current distribution is analyzed first for broadband excitation and second in the harmonic case.

A. Pulse Excitation

For broadband numerical analysis, the spiral is excited using a modulated Gaussian pulse with bandwidth covering the operation bandwidth of the device. Fig. 7 shows the instantaneous current density on the spiral arms at selected times for excitation with a single pulse (shown in the inset of Fig. 8). In the simplified model used for these representations, the feed is provided by a point source in the spiral center, to avoid pulse distortions caused by the balun. The most obvious feature of the propagation along the spiral arms is a temporal broadening of the pulse. This frequency dispersive behavior is explained classically by the radiation mechanism of the spiral: The energy associated to a certain frequency component is radiated from a ring-like region with a circumference approximately equal to a full wavelength [14]. Therefore, higher frequency components are radiated from regions located closer to the feed than lower frequency components. In the representation of Fig. 7, the current density has been normalized for each snapshot to the instantaneous maximum $J_{\max}$ which decays with time as shown in Fig. 8. It should be noted that the exact rate of the decay is dependent on the spectrum of the excitation pulse. The decay is interrupted after 8 ns because the leading components of the pulse have reached the end of the spiral and are reflected toward the feed.

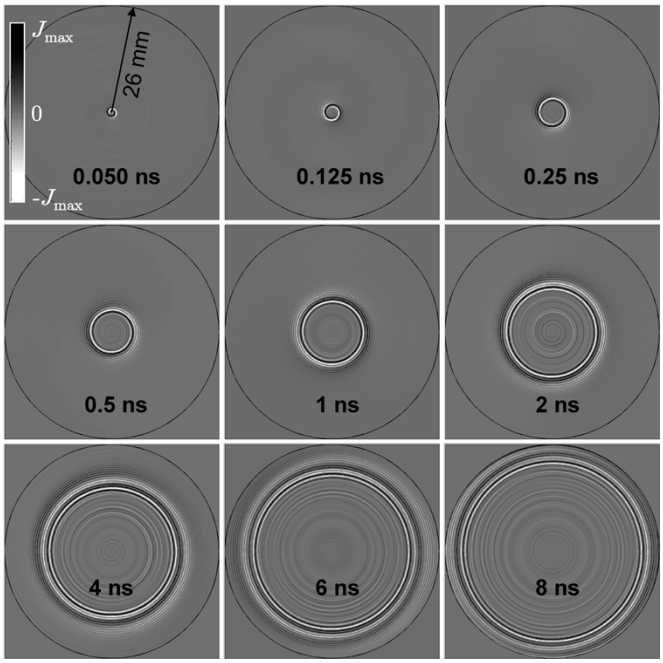

Fig. 7. Propagation of a single pulse on the spiral antenna. The outer circle indicates the maximum radius of the spiral. Each plot is a snapshot of the current density distribution normalized to the instantaneous maximum current density $J_{\max}(t)$. The contrast is exaggerated for better visibility. The sign of the current density is defined by considering the propagation direction along the spiral.

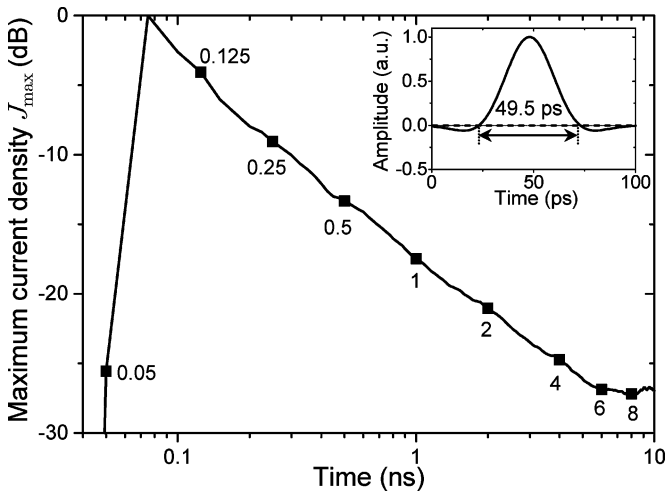

Fig. 8. Maximum of the current density on the spiral as a function of time (in logarithmic scale). The filled squares indicate the times corresponding to the images of Fig. 6. As the pulse propagates along the spiral, the maximum current density decays because of radiation. The higher frequency components are radiated first. Inset: shape of the pulse used for excitation.

The temporal evolution of the pulse is shaped by the frequency-dependent radiation process, but is also influenced by the crosstalk between the adjacent windings of the spiral in radial direction. This can be anticipated looking at Fig. 7 but becomes clearly visible in the representation of Fig. 9. There, instantaneous current densities along the length of one arm of the spiral are represented at several times of the simulation. Only 1.0 m of the 2.2 m total length of the spiral arm is represented. Also indicated in the top scale are the starts of new spiral turns.

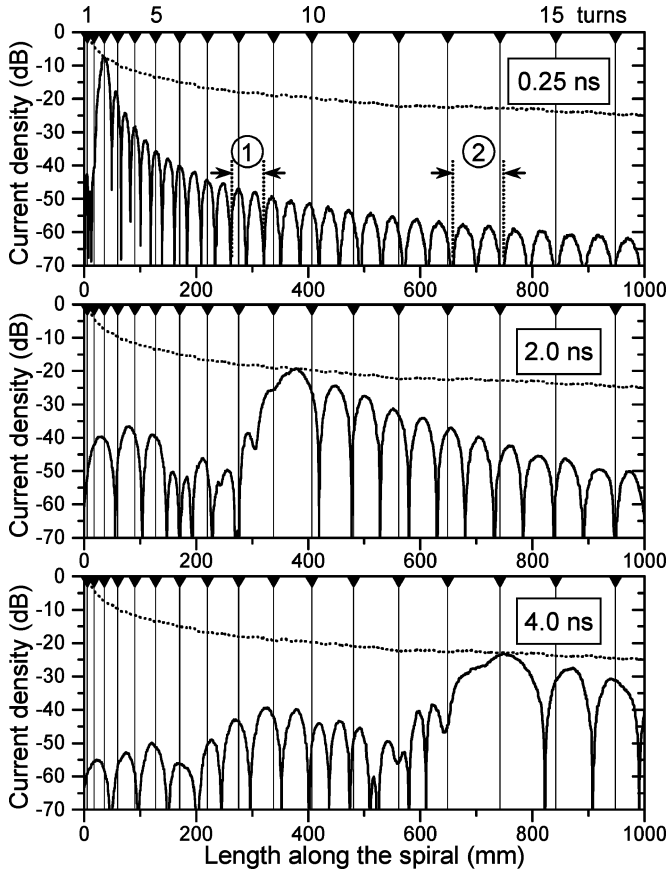

Fig. 9. Current density distribution of a pulse propagating along one arm of the spiral at three different times. Each graph shows the envelope of the current density (dotted line) as well as the instantaneous current density at the indicated time (solid line). The length along the arm is measured in the middle of the spiral metallization. As the short pulse propagates along the spiral, it becomes broadened and its amplitude decays. Also visible are oscillations (ringing) caused by coupling between adjacent windings of the spiral arms.

Several characteristics of the pulse propagation on the spiral can be highlighted.

- The pulse broadening and amplitude decay are clearly visible in this representation.
- The maximum of the pulse shows propagation velocity smaller than the free-space velocity along the spiral. This is partly explained by the influence of the substrate. It is also postulated that current-wave propagation is not constant and dispersive along the spiral, causing lower frequencies to be slower in the inner turns of the spiral than higher frequency components. This results in the chirp of the pulse that is visible in the spatial domain along the arm of the spiral.
- Besides propagation of currents along the spiral arms, mutual coupling between the adjacent windings of the spiral represents another propagation path on the spiral, in radial direction. This becomes apparent in the oscillations (ringing) that extend to the outer windings of the spiral. The growth of the ringing width (especially visible in the upper graph of Fig. 9 comparing, e.g., the circled location 1 and 2) is caused by the increased length of the spiral turns toward the outer region.
- A low-amplitude wave is also observed in the inner turns of the spiral (left from the pulse maximum in the graphs),

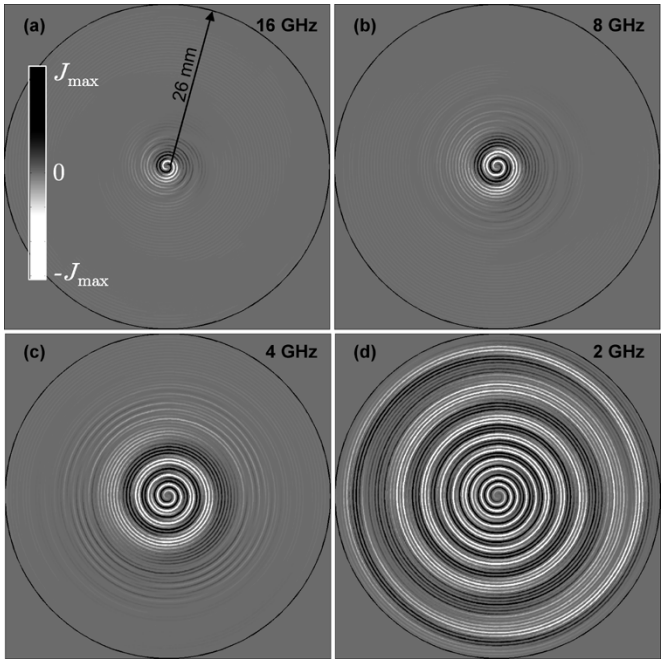

Fig. 10. Snapshots of the steady-state current density for different frequencies: (a) 16 GHz, (b) 8 GHz, (c) 4 GHz, (d) 2 GHz. The contrast is exaggerated for better visibility. The outer circle indicates the maximum radius of the spiral. The scale shown in (a) applies to the four images.

with components propagating from the maximum toward the center. The observed intricate patterns are formed both by reflections and crosstalk effects.

In summary, the propagation along the spiral arms is influenced by several effects: dispersion (chirp), crosstalk between the arms and reflection at the outer end of the spiral arms. The characteristics of the propagation can be better characterized using harmonic excitation, as described in the next section.

B. Harmonic Excitation

The use of monochromatic sinusoidal excitation permits a better visualization of the frequency dependence of the spiral radiation mechanism. The current density distribution on the spiral (printed on a substrate) at a particular time in steady-state is shown in Fig. 10 at the operation frequencies of 2, 4, 8 and 16 GHz. These images qualitatively demonstrate the concept of frequency-dependent active region where the radiation process is taking place on the Archimedean spiral: This active region adapts itself to the operation wavelength and is characterized by in-phase currents on two adjacent arms [14], which occurs in an annulus around the feed with a mid-radius equal to $\lambda_{\text{eff}}/2\pi$. The effective wavelength λ_{eff} is the wavelength of the waves on the spiral arms and is determined by the substrate characteristics, and by the geometry of the spiral.

The classical model considers damped sinusoidal currents on the spiral arms and describes qualitatively the frequency-dependent behavior of the spiral antenna. The simulations presented here permits a more detailed view of the current distribution on the spiral, taking into account the effect of the substrate and the mutual coupling between the windings.

Fig. 11 shows the amplitude of the current density as a function of the radial distance from the feed on the spiral arms at

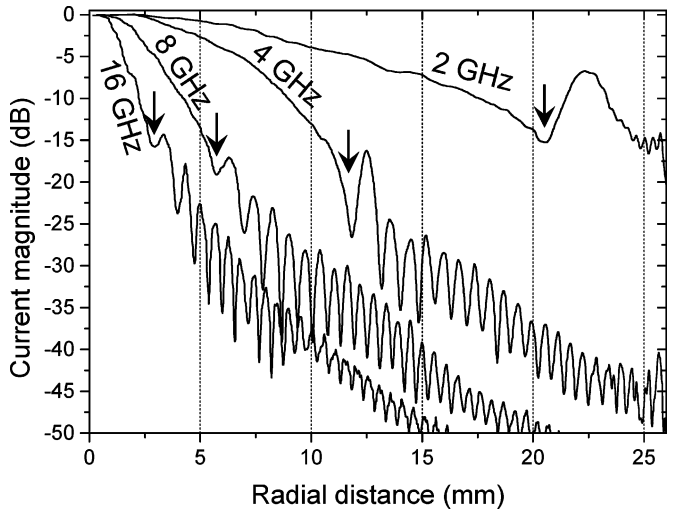

Fig. 11. Amplitude of the current density on the spiral arm as a function of the radial distance from the center for 4 frequencies of operation: 2, 4, 8 and 16 GHz.

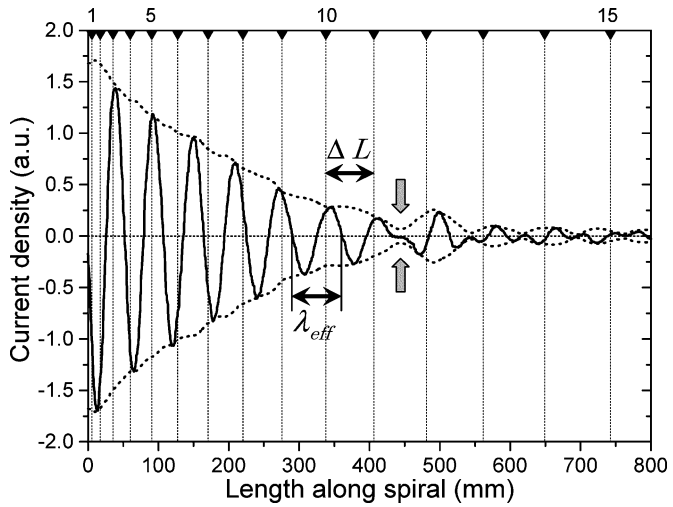

Fig. 12. Instantaneous current density along the arm of the Archimedean spiral for 4 GHz excitation. The envelope is also shown as dotted line. Only the first 800 mm of the 2200 mm spiral arms are displayed on the graph. The upper horizontal scale indicates the turns of the spiral. The length along the spiral is measured in the middle of the metallic arm.

2, 4, 8 and 16 GHz. The curves represent another illustration of the frequency-dependent current decay along the spiral arms. However, another distinctive characteristic can be observed in Fig. 11: A local minimum (highlighted by an arrow) is visible in each curve after the initial decay of the current along the spiral. Beyond this minimum, the amplitude is characterized by oscillations indicating a standing wave pattern. Therefore, this minimum is interpreted as an indicator of the outer limit of the active region of the spiral antenna.

Fig. 12 represents the simulated instantaneous current density at 4 GHz along one arm of the spiral. Also represented is the envelope of the current density along this arm. The distinctive minimum described in the previous paragraph is indicated by the arrows in the graph and can be used to define two domains:

- On the inner part of the spiral, before this minimum, the current density takes the shape of a damped sinusoid traveling outwards. However, the apparent wavelength of the

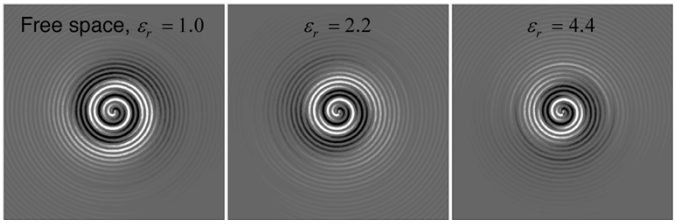

Fig. 13. Simulated instantaneous current density distribution at 8 GHz on the center of the spiral antenna for the spiral in free-space (left graph) as well as for two different values of the substrate dielectric permittivity. All images are plotted for the same time, i.e., with the same excitation phase. The side of the square area shown is equal to 24 mm.

oscillations along the arm varies slightly with the location on the spiral, because of the changing transverse field distribution. Shortly before the highlighted minimum, the observed effective wavelength λ_{eff} corresponds to a spiral turn ΔL, as highlighted in Fig. 12.

- On the outer turns of the spiral, beyond the minimum, the current distribution is no more sinusoidal and exhibits standing wave characteristics. The wave is shaped by crosstalk between the windings and by the reflection on the arms of the spiral.

Based on this consideration, the effective wavelength λ_{eff} in the active radiation region is retrieved from simulations, considering the observed wavelength on the inner spiral windings just preceding the distinctive minimum (i.e. around half-turn before). Based on this effective wavelength, the effective permittivity ε_{eff} in the active region can be estimated according to

$$\lambda_{\text{eff}} = \frac{\lambda_0}{\sqrt{\varepsilon_{\text{eff}}}} \tag{3}$$

and the radius of the active region corresponds then to

$$r_{\text{eff}} = \frac{\lambda_{\text{eff}}}{2\pi} = \frac{\lambda_0}{2\pi\sqrt{\varepsilon_{\text{eff}}}}. \tag{4}$$

The determination of these quantities permits to characterize the effect of the substrate below the spiral, as described in the following section.

C. Substrate Effects

The spiral described here is placed on a 0.254 mm thick substrate with permittivity $\varepsilon_r = 2.2$. The effect of this thin substrate on the current density is characterized by the effective permittivity in the active region and/or by the active radius of the spiral, according to (4). To illustrate the current density distribution variations caused by the substrate, the value ε_r is varied in a numerical experiment. Fig. 13 compares the current densities at 8 GHz for different permittivities of the substrate: $\varepsilon_r = 1$ (no substrate), $\varepsilon_r = 2.2$ (actual value of the substrate) and $\varepsilon_r = 4.4$. The images show clearly the shrinking of the active region caused by the increase of effective permittivity. This effect has been described in more detail in [15] and demonstrates that the thin substrate must be included in the simulation of the spiral antenna.

The value of the effective permittivity retrieved from the simulation is represented as a function of the frequency in Fig. 14.

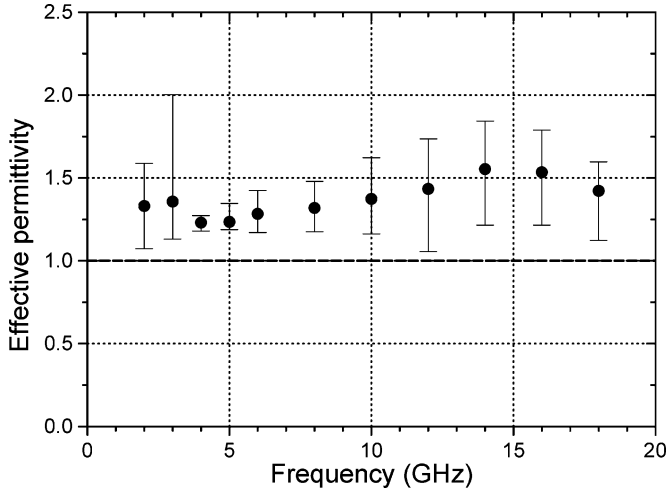

Fig. 14. Computed value of the effective permittivity on the spiral arms in the active radiating region. The error bars indicate the variations observed inside the considered region around the frequency-dependent active radius.

The uncertainty is caused by the variations of the effective wavelength along the spiral arms (in and around the active region) and is influenced by the reflections on the spiral arms. The average value (and standard deviation) of the relative permittivity for the given frequencies is found to be $\varepsilon_{\text{eff}} = 1.37 \pm 0.11$. The thin substrate with $\varepsilon_r = 2.2$ reduces then for a given frequency the active radiating radius of the spiral by 15–20%.

V. Conclusion

This paper has described the simulation and measurement of a broadband cavity-backed Archimedean spiral antenna. The presented results have addressed two complementary aspects: The numerical technique utilized in the simulation and the detailed analysis of the spiral antenna.

The FVTD method proved to be a valuable and effective tool for the simulation of the spiral antenna. The numerical results of the radiation and matching characteristics show a very good agreement with measured data, demonstrating the suitability of the method for complex multiple scale problems. The use of a tetrahedral mesh with a strong inhomogeneity permits to resolve the fine spiral structure, the thin substrate as well as the details of the feed with great fidelity. The modeling of those details has been shown to be relevant for the simulation of the overall structure.

Despite a relatively low memory requirement (1 GB for the full model), time-domain simulations of the spiral are still very costly in terms of CPU time: the pulse used for broadband excitation has to propagate all along the arms of the spiral antennas in order to achieve satisfying results down to the lower frequencies of operation. For the spiral antenna with an arm length of more than 2 m, this requires a time of around 10 ns in the simulation.

The current density distribution on the spiral antenna arms has been simulated both for pulsed and for harmonic excitation. This has provided a deeper insight into the radiation mechanism on the spiral antenna, including the coupling effect between the windings and the influence of the thin substrate. Although the current distribution is shown not to be strictly sinusoidal because

of coupling effects, an effective permittivity can be defined locally to describe the frequency-dependent extent of the active radiating region on the spiral.

REFERENCES

[1] H. Nakano, K. Nogami, S. Arai, H. Mimaki, and J. Yamauchi, "A spiral antenna backed by a conducting plane reflector," *IEEE Trans. Antennas Propag.*, vol. AP-34, pp. 1417–1423, Jun. 1986.

[2] U. Jakobus, J. Christ, and F. M. Landstorfer, "PO-MoM analysis of cavity-backed antennas," in *Proc. Inst. Elect. Eng. 8th Int. Conf. Antennas Propagat. ICAP'93*, Apr. 1993, pp. 111–114.

[3] C. W. Penney and R. J. Luebbers, "Input impedance, radiation pattern, and radar cross section of spiral antennas using FDTD," *IEEE Trans. Antennas Propag.*, vol. 42, pp. 1328–1332, Sep. 1994.

[4] J. Thaysen, K. B. Jakobsen, and J. Appel-Hansen, "Characterization and optimization of a coplanar waveguide fed logarithmic spiral antenna," in *Proc. IEEE APS Conf. Antennas Propagat. for Wireless Communications*, Nov. 2000, pp. 25–28.

[5] D. S. Filipović and J. L. Volakis, "Novel slot spiral antenna designs for dual-band/multiband operation," *IEEE Trans. Antennas Propag.*, vol. 51, pp. 430–440, Mar. 2003.

[6] M. N. Afsar, Y. Wang, and R. Cheung, "Analysis and measurement of a broadband spiral antenna," *IEEE Antennas Propag. Mag.*, vol. 46, pp. 59–64, Feb. 2004.

[7] H. Nakano, M. Ikeda, K. Hitosugi, and J. Yamauchi, "A spiral antenna sandwiched by dielectric layers," *IEEE Trans. Antennas Propagat.*, vol. 34, pp. 791–796, Jun. 2004.

[8] N. K. Madsen and R. W. Ziolkowski, "A three-dimensional modified finite volume technique for Maxwell's equations," *Electromagn.*, vol. 10, pp. 147–161, 1990.

[9] V. Shankar, A. H. Mohammadian, and W. F. Hall, "A time-domain, finite-volume treatment for the Maxwell equations," *Electromagn.*, vol. 10, pp. 127–145, 1990.

[10] K. S. Yee and J. S. Chen, "The finite-difference time-domain (FDTD) and the finite-volume time-domain (FVTD) methods in solving Maxwell's equations," *IEEE Trans. Antennas Propag.*, vol. 45, pp. 354–363, Mar. 1997.

[11] P. Bonnet, X. Ferrieres, B. L. Michielsen, P. Klotz, and J. L. Roumiguières, "Finite-volume time domain method," in *Time Domain Electromagnetics*, S. M. Rao, Ed. San Diego, CA: Academic Press, 1999, ch. 9.

[12] C. Fumeaux, D. Baumann, P. Leuchtmann, and R. Vahldieck, "A generalized local time-step scheme for efficient FVTD simulations in strongly inhomogeneous meshes," *IEEE Trans. Microwave Theory Tech.*, vol. 52, pp. 1067–1076, Mar. 2004.

[13] D. Baumann, C. Fumeaux, P. Leuchtmann, and R. Vahldieck, "Generalized-scattering-matrix extraction using the finite-volume time-domain (FVTD) method," in *IEEE MTT-S Int. Microwave Symp. Dig.*, Jun. 2004, pp. 1701–1704.

[14] J. A. Kaiser, "The Archimedean two-wire spiral antenna," *IRE Trans. Antennas Propag.*, vol. 8, pp. 312–323, May 1960.

[15] C. Fumeaux, D. Baumann, and R. Vahldieck, "FVTD simulations of Archimedean spiral antennas on thin substrates in planar and conformal configurations," in *IEEE/ACES Conf. Wireless Communications and Appl. Comp. Electromagnetics*, Apr. 2005, pp. 277–280.

Christophe Fumeaux (M'03) received the Diploma and Ph.D. degrees in physics from the Swiss Federal Institute of Technology (ETH), Zürich, Switzerland, in 1992 and 1997, respectively.

From 1998 to 2000, he was a Postdoctoral Researcher involved in infrared technology with the School of Optics, University of Central Florida, Orlando. In 2000, he joined the Swiss Federal Office of Metrology, Bern, Switzerland, as a Scientific Staff Member. Since 2001, he has been a Research Associate with the Laboratory for Electromagnetic Fields and Microwave Electronics (IFH), ETH, Zürich, Switzerland. During Fall 2005, he was a Visiting Scientist with the Laboratory of Sciences and Materials for Electronics, and of Automatic (LASMEA), University Blaise Pascal, Clermont-Ferrand, France. His current main research interest concerns computational electromagnetics in the time domain for numerical analysis of microwave circuits and antennas.

Dr. Fumeaux was the recipient of the ETH Silver Medal of Excellence for his doctoral dissertation, and was the co-recipient of the ACES outstanding paper award in 2004.

Dirk Baumann (S'01) received the Dipl. Ing. degree in electrical engineering from the University of Karlsruhe, Germany, in 2001. Currently he is working toward the Ph.D. degree in electrical engineering at the Laboratory for Electromagnetic Fields and Microwave Electronics (IFH), ETH Zurich, Switzerland.

Between Spring and Fall 2000 he did an internship at the Alaska SAR Facility (ASF), Fairbanks, AK, working on the calibration of ASF's SAR processor. His research interests include numerical methods with emphasis on time domain techniques and their application to general electromagnetic problems.

Mr. Baumann was the co-recipient of the ACES outstanding paper award in 2004.

Rüdiger Vahldieck (M'85–SM'86–F'99) received the Dipl.-Ing. and Dr.-Ing. degrees in electrical engineering from the University of Bremen, Bremen, Germany, in 1980 and 1983, respectively.

From 1984 to 1986, he was a Postdoctoral Fellow at the University of Ottawa, ON, Canada. In 1986, he joined the Department of Electrical and Computer Engineering at the University of Victoria, British Columbia, Canada, where he became a Full Professor in 1991. During Fall and Spring of 1992–1993 he was a Visiting Scientist at the "Ferdinand-Braun-Institut für Höchstfrequenztechnik" in Berlin, Germany. In 1997, he became a Professor for electromagnetic field theory at the Swiss Federal Institute of Technology, Zurich, Switzerland, and became Head of the Laboratory for Electromagnetic Fields and Microwave Electronics (IFH) in 2003. Since 2005, he is also the Head of the Department of Information Technology and Electrical Engineering (D-ITET). Since 1981, he has published more than 230 technical papers in books, journals and conferences, mainly in the field of microwave CAD. His research interests include computational electromagnetics in the general area of EMC and in particular for computer-aided design of microwave, millimeter wave and optoelectronic integrated circuits.

Prof. Vahldieck received the J. K. Mitra Award of the Institution of Electronics and Telecommunication Engineers (IETE) for the Best Research Paper in 1995. He was co-recipient of the outstanding publication award of the Institution of Electronic and Radio Engineers in 1983, and of the ACES outstanding paper award in 2004. He is the Past-President of the IEEE 2000 International Zurich Seminar on Broadband Communications (IZS'2000) and since 2003 President and General Chairman of the international Zurich Symposium on Electromagnetic Compatibility. He is a member of the editorial board of the IEEE TRANSACTION ON MICROWAVE THEORY AND TECHNIQUES. From 2000 to 2003, he served as an Associate Editor for the IEEE MICROWAVE AND WIRELESS COMPONENTS LETTERS, and from 2003 to 2005, was Editor-in-Chief. Since 1992, he is on the Technical Program Committee of the IEEE International Microwave Symposium and the MTT-S Technical Committee on Microwave Field Theory. From 1998 until 2003, he was the Chapter Chairman of the IEEE Swiss Joint Chapter on MTT, AP and EMC. In 2005, he became President of the Swiss Research Foundation on Mobile Communication.